

# Decentralized Uncertainty-Aware Active Search with a Team of Aerial Robots

Wennie Tabib, John Stecklein, Caleb McDowell, Kshitij Goel, Felix Jonathan, Abhishek Rathod, Meghan Kokoski, Edsel Burkholder, Brian Wallace, Luis Ernesto Navarro-Serment, Nikhil Angad Bakshi, Tejus Gupta, Norman Papernick, David Guttendorf, Erik E. Kahn, Jessica Kasemer, Jesse Holdaway, and Jeff Schneider



Fig. 1: Active search by a team of two aerial robots. (a) Image taken of one robot during flight. (b) The flight paths for each robot are shown in red and green plotted on top of a georegistered mesh. Unexplored cells are opaque and explored cells are transparent. The safe flight area is outlined in red. A video of this experiment may be found at <https://youtu.be/lzh8M134enw>. A video of active search conducted with three robots may be found at <https://youtu.be/xgLnS2IFCQQ>.

**Abstract**—Rapid search and rescue is critical to maximizing survival rates following natural disasters. However, these efforts are challenged by the need to search large disaster zones, lack of reliability in the communications infrastructure, and *a priori* unknown numbers of objects of interest (OOIs), such as injured survivors. Aerial robots are increasingly being deployed for search and rescue due to their high mobility, but there remains a gap in deploying multi-robot autonomous aerial systems for methodical search of large environments. Prior works have relied on preprogrammed paths from human operators or are evaluated only in simulation. We bridge these gaps in the state of the art by developing and demonstrating a decentralized active search system, which biases its trajectories to take additional views of uncertain OOIs. The methodology leverages stochasticity for rapid coverage in communication denied scenarios. When communications are available, robots share poses, goals, and OOI information to accelerate the rate of search. Extensive simulations and hardware experiments in Bloomingdale, OH, are conducted to validate the approach. The results demonstrate the active search approach outperforms greedy coverage-based planning in communication-denied scenarios while maintaining comparable performance in communication-enabled scenarios.

\*The authors are with the Robotics Institute, Carnegie Mellon University, Pittsburgh, PA 15213 USA. (email: {wtabib, jsteckle, cmcdowel, kgoel1, fjonatha, arathod2, mkokoski, eburkhol, luisn, nabakshi, tejug, norm, davidg, eekahn, jkasemer, jholdawa, jeff4}@andrew.cmu.edu.)

## I. INTRODUCTION

Rapid emergency response is key to maximizing the survival rate following a disaster. Rescuing a victim within the first 24 hours yields a survival rate of 90%, which drops precipitously to 5-10% after 72 hours [1]. Due to their speed, agility, and maneuverability in challenging three dimensional environments, unmanned aerial systems are increasingly being deployed to facilitate search and rescue [2]. For example, in 2014 a drone pilot was able to locate an 82 year old man in 20 minutes after rescue teams searched unsuccessfully over a three day period [2, 3].

When the number of victims is *a priori* unknown, which is often the case after natural disasters (e.g., hurricanes), automated methods are needed to systematically and methodically cover the disaster area. After Hurricane Harvey, Fernandes et al. [4] conducted 112 preprogrammed and remotely piloted flights. Each flight required 2-3 people for support. We would like to develop automated methods of search that reduce the reliance on operators and pilots to coordinate teams of aerial robots. Because wireless communication and mobile phones are often unusable post-disaster (e.g.,

Hurricane Katrina) [5] or jammed [6], the multi-agent search methods should be robust to communication dropouts and failures.

The problem this work seeks to address is how to autonomously and rapidly search an area to discover objects of interest (OOIs), such as injured persons. We develop a decentralized, multi-agent reinforcement learning approach for active search that utilizes cross-robot communication when available, is robust to communication dropouts, and adapts the behavior of the agents to take additional views of areas when detection uncertainty is high.

## II. RELATED WORKS

This section reviews recent works in autonomy for search and environment monitoring, and contrasts with the proposed approach.

Stache et al. [7] develop an environment monitoring system, which uses a Gaussian Process as a decision function, to modulate an aerial robot’s altitude according to the accuracy of semantic segmentation. The objective is to maximize the classification accuracy of objects in the images. The initial plan creates a set of waypoints at a fixed altitude in a lawnmower pattern [8]. The decision function outputs the next waypoint, which may vary the altitude, based on an input waypoint and the result of semantic segmentation. When the altitude is changed, the GP is updated. While the approach is evaluated in post-processing, it is not evaluated with real-world experiments. In contrast, our active search methodology is demonstrated with a team of three aerial robots in real world experiments.

Meera et al. [9] develop an obstacle-aware informative path planning solution for target search. A GP is used to represent the 2D ground plane; however, it is discretized and sensor measurements are fused by using the field of view of the onboard camera to determine which cells are within the view (as well as occlusions from a 3D Euclidean Signed Distance Field). The field map is updated using a Kalman filter. Evaluations are conducted in simulation only.

Horyna et al. [10] leverage multi-agent flocking behaviors to increase the reliability of OOI detection. When an OOI is detected, one of the members from the swarm may separate to confirm the detection. In contrast, the team of robots in the proposed approach does not maintain a formation. The reward function enables reflexes over uncertain OOIs while maximizing coverage of the space. A limitation of the approach by Horyna et al. [10] is that sweeping trajectories are manually set by a human. These trajectories are executed when no object is being approached by the swarm. In contrast, the operator defines an operational zone in our approach and the agents autonomously determine where to search in a decentralized manner. Because the swarms in [10] operate in close proximity to one another the maximum speed during hardware experiments is set to 1 m/s. In contrast, our approach exceeds speeds of 10 m/s. The maximum area for [10] is 6400 m<sup>2</sup> whereas ours is approximately one order of magnitude larger at 72 000 m<sup>2</sup>.

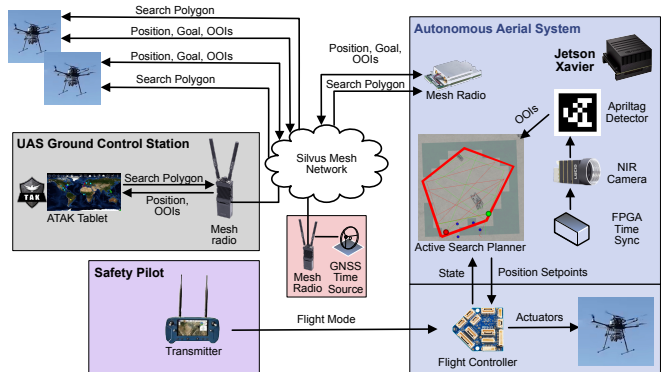


Fig. 2: System diagram for the active search approach. An operator uses the Android Team Awareness Kit (ATAK) app on a tablet to draw a convex polygon of an area for the aerial systems to search. The polygon is sent to one or more robots over a Silvus mesh radio. Safety pilots launch the vehicles. All search operations are conducted without human intervention. The robot receives state information from the flight controller and camera images are processed to localize objects of interest (OOIs) on the ground below. The planner sends position setpoints to the flight controller, which are used to send actuator commands to the motors. When communications are enabled, the robot transmits position, target, and goal information to other robots. A universal time synchronizer synchronizes time between robots when communications are enabled. When the battery is depleted, the robots return to their takeoff locations and the safety pilots land their vehicles.

## III. CONTRIBUTIONS

We extend prior work by Bakshi et al. [11], which leverages Thompson Sampling, for active search and provide the following contributions. First, we provide analysis for a multi-agent aerial team in real-world experiments whereas [11] deployed only a single aerial vehicle. We also incorporate goals from other robots when planning the next best action and provide an analysis of coverage as a function of time, which is important when the number of OOIs is *a priori* unknown. The effects of communication are analyzed in real-world hardware trials and the OOI localization accuracy is also reported. Finally, we provide an efficient C++ implementation of the active search algorithm with Python bindings for ease of prototyping and deployment to hardware<sup>1</sup>.

## IV. METHODOLOGY

This section provides an overview of the multirobot active search system, which enables a team of aerial robots to select views that search the environment, detect OOIs, and bias trajectories to collect additional views of uncertain OOIs while remaining robust to communication failures. Fig. 2 provides a system diagram for the active search approach. The active search algorithm is detailed in Sections IV-A and IV-B. The trajectory generation method and interaction with the flight controller is discussed in Section IV-C. The hardware configuration is detailed in Section IV-D.

*a) Notation:* In this paper, lowercase boldface symbols represent column vectors (e.g.,  $\mathbf{b}$ ). The  $i$ th entry of a vector  $\mathbf{b}$  is denoted as  $b_i$ . Uppercase bold letters (e.g.,  $\mathbf{B}$ ) represent matrices or sets. Sets and matrices may have the subscript  $\mathbf{B}_{a:b}$ , which means that the matrix or set is composed of data (e.g., row vectors or scalars) from timestamp  $a$  through

<sup>1</sup><https://github.com/rislab/guts-sandbox>

timestamp  $b$ , inclusive. The transpose of a matrix  $\mathbf{B}$  is denoted as  $\mathbf{B}^\top$ . A square matrix with nonzero entries  $\mathbf{b}$  along the diagonal is represented as  $\text{diag}(\mathbf{b})$ . The  $\ell_2$ -norm of a vector  $\mathbf{b}$  is written as  $\|\mathbf{b}\|_2$ . Where it is important to denote that a particular value is maintained by robot  $j$ , it is written as a superscript (i.e.,  $\mathbf{b}^j$ ).

#### A. Active Search

This section details the active search methodology for a single robot (i.e., the communication-denied scenario). It is extended to the communication-enabled case in the next section. The environment is a 2D discrete representation of dimension  $M = M_w \times M_h$ , which may be flattened into a vector,  $\boldsymbol{\beta} \in \mathbb{R}^M$ .  $\mathbf{x}_i \in \mathbb{R}^{1 \times M}$  is a one-hot sensing row vector. The aerial system sensing action model consists of all the cells along the straight line between a start and end point. Therefore, an action may be represented using multiple sensing row vectors. Robot positions and OOI detection locations are encoded in  $\mathbf{x}_i$  with 1. All other entries are 0. Each robot also maintains a scalar value  $y_i$ , which represents the output of the object detector as well as the OOI confidence,  $c_i$ .

The data  $\mathbf{D}_{1:i} = \{(\mathbf{x}_1, y_1), \dots, (\mathbf{x}_i, y_i)\}$  consists of all sensor row vectors and observations up to timestep  $i$ . The sensor row vectors are vertically stacked to create a matrix  $\mathbf{X}_{1:i}$  and observations  $y_i$  are also vertically stacked to create a column vector  $\mathbf{y}_{1:i}$ . For example, if  $\mathbf{D}_{1:3} \equiv \{(\mathbf{x}_1, y_1), (\mathbf{x}_2, y_2), (\mathbf{x}_3, y_3)\}$ , then  $\mathbf{X}_{1:3} = [\mathbf{x}_1 \ \mathbf{x}_2 \ \mathbf{x}_3]^\top$  and  $\mathbf{y}_{1:3} = [y_1 \ y_2 \ y_3]^\top$ . Noise is modeled with a diagonal matrix  $\boldsymbol{\Sigma}_{1:i} = \text{diag}([\sigma_1^2 \ \dots \ \sigma_i^2]^\top)$ , where  $\sigma_i^2 = \frac{1}{c_i}$ .

Expectation Maximization is used to estimate the posterior distribution of  $\boldsymbol{\beta}$  given data  $\mathbf{D}_{1:i}$ ,  $p(\boldsymbol{\beta}|\mathbf{D}_{1:i}, \boldsymbol{\Gamma}) = \mathcal{N}(\boldsymbol{\mu}, \mathbf{V})$ , where  $\boldsymbol{\mu}$  and  $\mathbf{V}$  are defined as

$$\begin{aligned} \mathbf{V} &= (\boldsymbol{\Gamma}^{-1} + \mathbf{X}_{1:i}^\top \boldsymbol{\Sigma}_{1:i} \mathbf{X}_{1:i})^{-1} \\ \boldsymbol{\mu} &= \mathbf{V} \mathbf{X}_{1:i}^\top \boldsymbol{\Sigma}_{1:i} \mathbf{y}_{1:i} \end{aligned}$$

and where  $\boldsymbol{\Gamma} \in \text{diag}([\gamma_1 \ \dots \ \gamma_M]^\top)$  are the hidden variables [11, 12]. It should be noted that  $\boldsymbol{\Gamma} \in \mathbb{R}^{M \times M}$  and  $\boldsymbol{\mu} \in \mathbb{R}^M$ .

The Maximization step maximizes the likelihood of  $p(\mathbf{y}_{1:i}|\boldsymbol{\Gamma}, \mathbf{X}_{1:i})$  such that the responsibilities  $\gamma_m$ , where  $m \in [1, \dots, M]$ , may be calculated as:

$$\gamma_m = ([\mathbf{V}]_{mm} + [\boldsymbol{\mu}]_m^2 + 2b_m)/(1 + 2a_m).$$

$a_m = 0.1$  and  $b_m = 1$  in keeping with [11, 12]. After these operations are complete, the robot samples from the posterior  $\boldsymbol{\beta} \sim p(\boldsymbol{\beta}|\mathbf{D}_{1:i})$ .

To select the next sensing action  $\mathbf{X}_{i+1:n} = [\mathbf{x}_{i+1} \ \dots \ \mathbf{x}_n]^\top$ , which lies along a straight line trajectory to a candidate goal location, each agent minimizes the loss function  $\mathcal{L}(\tilde{\boldsymbol{\beta}}, \mathbf{D}_{1:i}, \mathbf{X}_{i+1:n})$

$$\mathcal{L}(\tilde{\boldsymbol{\beta}}, \mathbf{D}_{1:i}, \mathbf{X}_{i+1:n}) = \|\tilde{\boldsymbol{\beta}} - \hat{\boldsymbol{\beta}}\|_2 + \lambda I(\tilde{\boldsymbol{\beta}}, \hat{\boldsymbol{\beta}}) \quad (1)$$

where  $I(\tilde{\boldsymbol{\beta}}, \hat{\boldsymbol{\beta}})$  is an indicator function (defined in Eq. (8)), which encourages the selection of actions that may detect

targets outside the most confident set in the sample from the belief,  $\hat{\boldsymbol{\beta}}$ .  $\tilde{\boldsymbol{\beta}}$  is calculated as

$$\hat{\boldsymbol{\beta}} = \mathbf{H}_i \mathbf{y}_{1:i} + \mathbf{H}_n \mathbf{X}_{i+1:n} \tilde{\boldsymbol{\beta}} \quad (2)$$

$$[\mathbf{H}_i \ \mathbf{H}_n] = \mathbf{S}([\mathbf{X}_{1:i}^\top \boldsymbol{\Sigma}_{1:i} \ \mathbf{X}_{i+1:n}^\top \boldsymbol{\Sigma}_{i+1:n}]) \quad (3)$$

$$\mathbf{S} = \text{diag}((\mathbf{U}_{k,k})^{-1}) \quad (4)$$

$$\begin{aligned} \mathbf{U} &= ((\mathbf{X}_{1:i}^\top \boldsymbol{\Sigma}_{1:i} \mathbf{X}_{1:i} + \boldsymbol{\Gamma}^{-1}) \\ &\quad + \mathbf{X}_{i+1:n}^\top \boldsymbol{\Sigma}_{i+1:n} \mathbf{X}_{i+1:n}) \odot \mathbb{I} \end{aligned} \quad (5)$$

$\odot$  denotes elementwise multiplication and  $\mathbb{I}$  represents the identity matrix. In Eq. (4), the notation  $\text{diag}((\mathbf{U}_{k,k})^{-1})$  represents extracting the diagonal entries of the matrix  $\mathbf{U}$ , taking the inverse of these entries, and converting the column vector into a diagonal matrix.

$I(\tilde{\boldsymbol{\beta}}, \hat{\boldsymbol{\beta}})$  is determined by finding half the maximum value of  $\hat{\boldsymbol{\beta}}$  and  $\tilde{\boldsymbol{\beta}}$ , checking if the corresponding value of  $\hat{\beta}_k$  and  $\tilde{\beta}_k$  is larger, respectively, and then rounding to the nearest integer (0 or 1). If all elements of  $\hat{\mathbf{a}}$  match all elements of  $\tilde{\mathbf{a}}$ , then the indicator function specified in Eq. (8) returns a 0 and 1, otherwise.

$$\hat{a}_k = \lfloor \hat{\beta}_k > \max(\hat{\boldsymbol{\beta}})/2 \rfloor \quad (6)$$

$$\tilde{a}_k = \lfloor \tilde{\beta}_k > \max(\tilde{\boldsymbol{\beta}})/2 \rfloor \quad (7)$$

$$I(\tilde{\boldsymbol{\beta}}, \hat{\boldsymbol{\beta}}) = \begin{cases} 0, & \text{if } \hat{a}_k = \tilde{a}_k, \forall k \\ 1, & \text{otherwise} \end{cases} \quad (8)$$

$\lambda = 0.01$  in keeping with [11, 13].

#### B. Decentralized Multirobot Planning

This section details how the active search loss function changes when multiple robots share position, goal, and OOI information. Positions, goals, and tracks from other robots are incorporated through updates to the  $\mathbf{X}_{1:i}$  and  $\mathbf{y}_{1:i}$  variables. We will consider what happens to these variables when robot  $j$  receives information from robot  $k$ .

When robot  $j$  receives location information from robot  $k$ , robot  $j$  generates a sensor row vector  $\mathbf{x}_{i+1}^k$  and observation scalar  $y_{i+1}^k$  and appends it to the variables  $\mathbf{X}_{1:i}$  and  $\mathbf{y}_{1:i}$  as in the following equations:

$$\begin{aligned} \mathbf{X}_{1:i+1} &= [\mathbf{x}_1^j \ \dots \ \mathbf{x}_i^j \ \mathbf{x}_{i+1}^k]^\top \\ \mathbf{y}_{1:i+1} &= [y_1^j \ \dots \ y_i^j \ y_{i+1}^k]^\top. \end{aligned}$$

The same update is used when robot  $j$  receives an OOI detection from robot  $k$ .

When goals are transmitted, the update is slightly different because there are multiple cells that robot  $k$  traverses. If robot  $j$  has received information that robot  $k$  is at the position encoded in  $\mathbf{x}_{i+1}^k$ , and the next sensing action for robot  $k$  may be specified as  $\mathbf{X}_{i+2:n}^k = [\mathbf{x}_{i+2}^k \ \dots \ \mathbf{x}_n^k]^\top$ , then robot  $j$  appends to the variables  $\mathbf{X}_{1:i+1}$  and  $\mathbf{y}_{1:i+1}$  in the following way:

$$\begin{aligned} \mathbf{X}_{1:p} &= [\mathbf{x}_1^j \ \dots \ \mathbf{x}_i^j \ \mathbf{x}_{i+1}^k \ \mathbf{x}_{i+2}^k \ \dots \ \mathbf{x}_p^k]^\top \\ \mathbf{y}_{1:p} &= [y_1^j \ \dots \ y_i^j \ y_{i+1}^k \ y_{i+2}^k \ \dots \ y_p^k]^\top. \end{aligned}$$



Fig. 3: The aerial system takes off during an experiment at the test site in Bloomingdale, OH.

$\mathbf{D}_{1:p}^j = (\mathbf{X}_{1:p}, \mathbf{y}_{1:p})$  is used in Eq. (1) in place of  $\mathbf{D}_{1:i}$  since it contains all the information available to robot  $j$ . Formulating  $\mathbf{D}_{1:p}^j$  such that it includes goal information from other robots ensures that robot  $j$  will avoid visiting the same locations.

### C. Trajectory Design and Tracking

Because the hexarotor aerial system used in this work is differentially flat [14], single axis trajectories for  $x$ ,  $y$ ,  $z$  position as well as heading ( $\psi$ ) may be formulated for the robot to track between waypoints. We leverage the single-axis trajectory generation solution of [15] because it is computationally efficient on size, weight, and power constrained aerial systems (i.e., thousands of trajectories may be calculated per second). It also enables the time-parameterized calculation of position setpoints, which enables re-planning in flight using all available information up to  $\Delta t$  seconds before reaching the next waypoint. We briefly restate the approach of [15] and how it is used to create dynamically feasible trajectories.

Let  $s(t)$  represent a fifth-order polynomial trajectory for a single axis (ie,  $x$ ,  $y$ ,  $z$ , or  $\psi$ ), which is parameterized by time,  $t$ . Position setpoints may be calculated from  $s(t)$ , which has fully defined initial position  $p_0$ , velocity  $v_0$ , and acceleration  $a_0$  constraints as well as final position  $p_f$ , velocity  $v_f$ , and acceleration  $a_f$  constraints. The trajectory is valid in the interval  $t \in [0, \dots, T]$ . To obtain a position setpoint at  $t$ , we must calculate the value of  $s(t)$ , which is defined as

$$s(t) = \frac{\alpha}{120}t^5 + \frac{\kappa}{24}t^4 + \frac{\eta}{6}t^3 + \frac{a_0}{2}t^2 + v_0t + p_0. \quad (9)$$

and where  $\alpha$ ,  $\kappa$ , and  $\eta$  may be calculated in closed form using Eqs. (10) and (11).

$$\begin{bmatrix} \alpha \\ \kappa \\ \eta \end{bmatrix} = \frac{1}{T^5} \begin{bmatrix} 720 & -360T & 60T^2 \\ -360T & 168T^2 & -24T^3 \\ 60T^2 & -24T^3 & 3T^4 \end{bmatrix} \begin{bmatrix} \Delta p \\ \Delta v \\ \Delta a \end{bmatrix}. \quad (10)$$

$\Delta p$ ,  $\Delta v$ , and  $\Delta a$  may be calculated as

$$\begin{bmatrix} \Delta p \\ \Delta v \\ \Delta a \end{bmatrix} = \begin{bmatrix} p_f - p_0 - v_0T - \frac{1}{2}a_0T^2 \\ v_f - v_0 - a_0T \\ a_f - a_0 \end{bmatrix}. \quad (11)$$

The first, second and third derivatives of Eq. (9) may be calculated to obtain time-parameterized equations for velocity, acceleration, and jerk. The roots of the derivative of a given polynomial are the times at which the polynomial achieves a critical point, which can be used to ensure the vehicle limits are not exceeded.

### D. Aerial System Hardware Configuration

The aerial system platform is an Inspired Flight 1200 with dimensions  $1.4 \text{ m} \times 1.3 \text{ m} \times 0.7 \text{ m}$  (see Fig. 3). It uses a ModalAI<sup>4</sup> flight controller running a closed-source fork of the ModalAI firmware tag v1.11.3-0.2.3<sup>5</sup>, which is a modified version of the PX4 Autopilot firmware. The platform is equipped with a custom payload consisting of a NVIDIA Jetson AGX Xavier computer.

The sensing payload consists of a global shutter Lucid Vision Phoenix NIR camera, Lucid Vision Phoenix RGB camera, and Teledyne Calibir GX camera. The NIR camera is used for Apriltag detection in the hardware experiments. All cameras face at approximately  $45^\circ$  to the ground and communicate with the onboard computer via GigE. Silvus Technologies' StreamCaster 4240 mesh radios enable communications between aerial systems and operators via a mobile ad hoc network. The mesh network enables the aerial systems to automatically and dynamically route information between one another and intermediate participating radios (e.g., ground control stations, participating operators, and dedicated relay points). A tablet running geospatial mapping software called the Android Team Awareness Kit (ATAK) is on the network and transmits zone information to the aerial systems. The aerial systems transmit their poses and object detections to be visualized on the tablet.

## V. EXPERIMENTAL DESIGN AND RESULTS

### A. Simulation Results

The approach was tested in simulation on a Lenovo Thinkpad X1 with an 11th Gen Intel Core i7-1165G7

<sup>4</sup>[https://docs.px4.io/main/en/flight\\_controller/modalai\\_fc\\_v1.html](https://docs.px4.io/main/en/flight_controller/modalai_fc_v1.html)

<sup>5</sup><https://github.com/modalai/px4-firmware/releases/tag/v1.11.3-0.2.3>



Fig. 4: The (a) WingtraOne<sup>2</sup> VTOL is used to collect images of the test site and produce a (b) high-resolution, geo-registered point cloud and mesh of the environment using the Pix4DMatic<sup>3</sup> photogrammetry software. (c) illustrates a view from the WingtraOne. This image is the test set up for the results shown in Fig. 11.

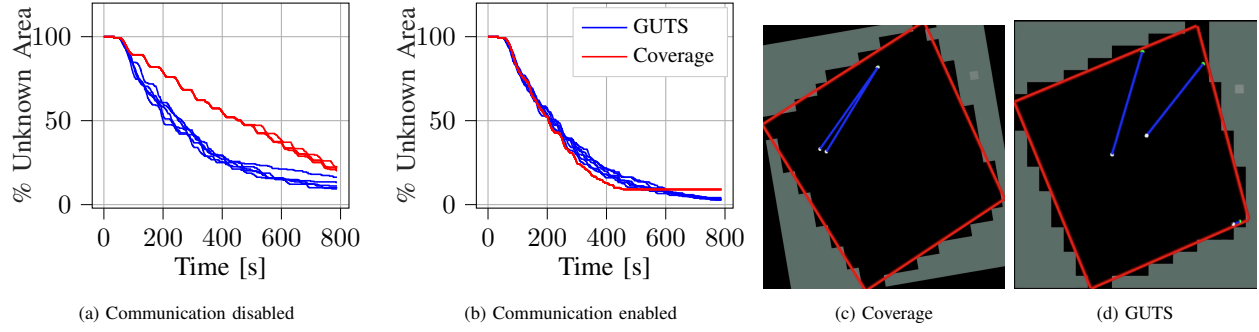


Fig. 5: Simulation results of three robots with and without communication enabled between robots. The performance of the GUTS planner is compared to a coverage planner. The results highlight that the stochasticity of the GUTS planner provides better coverage when (a) communications are disabled between drones as compared to the coverage planner, which is deterministic. (b) The GUTS planner suffers only slight performance decrease as compared to the coverage planner when communication is enabled. Each approach is run five times for 800s for a total of 20 trials.

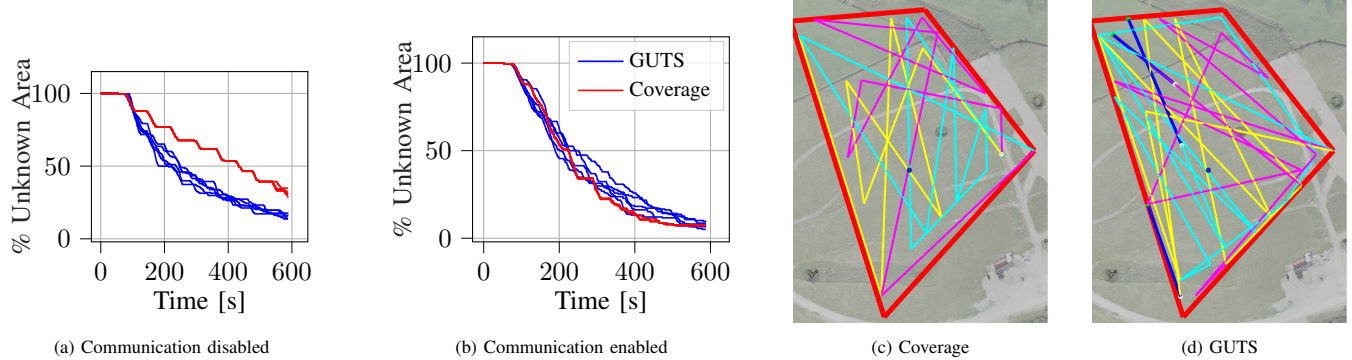


Fig. 6: Simulation results of three robots (a) with and (b) without communication enabled between aerial systems. The coverage results are similar to those in Fig. 5. An object of interest is illustrated as a blue dot in (c) and (d). The robot trajectories are shown in magenta, yellow, and cyan in both figures. The blue trajectories are the ones currently being executed in the simulation. The coverage image (c) has no blue trajectories because the robots have covered the entire area and have no waypoints left to select. The GUTS planner, in contrast, will continue executing trajectories.

2.8 GHz CPU, 4 cores (8 hyperthreads), and 16 GB RAM running Ubuntu 20.04. Because the Thompson Sampling approach is stochastic, multiple trials were run to better analyze the performance of the approach. The approach is compared to a deterministic coverage planner that greedily maximizes the amount of area visited when selecting waypoints. The results are analyzed by plotting the percent reduction in unknown area as a function of time. For each approach illustrated in Fig. 5 two cases are considered: communica-

tion disabled and communication enabled. The Thompson Sampling approach, labeled Generalized Uncertainty-Aware Thompson Sampling (GUTS), is illustrated as blue lines and the greedy coverage planner is illustrated in red. In the communication-denied scenario, we see that the GUTS approach outperforms the coverage-based approach due to the stochasticity. The coverage approach in the communication enabled case (Fig. 5b) slightly outperforms the GUTS approach early on; however, towards the end of the run

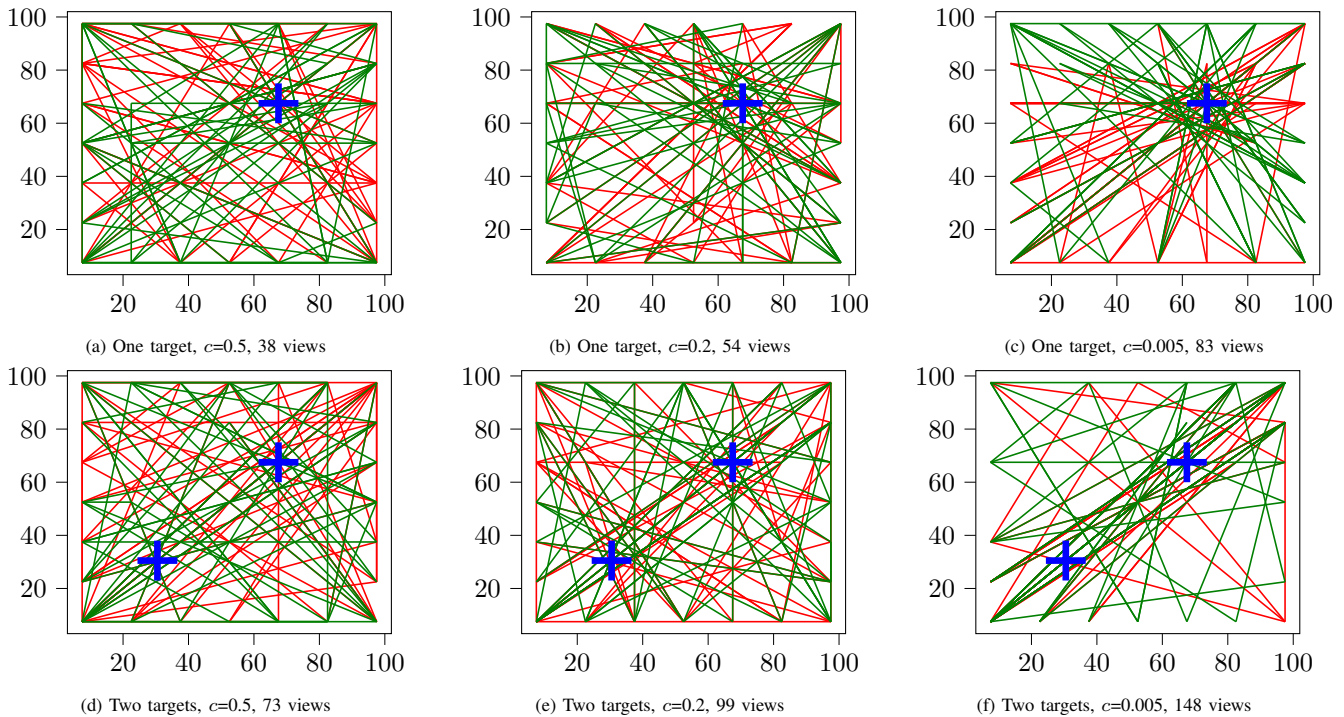


Fig. 7: Simulation results that provide qualitative and quantitative example of the effect of varying  $c$  for a team of two robots. The location(s) of the target(s), or object(s) of interest is shown as a blue cross(es). The trajectory for robot 1 is shown in red and the trajectory for robot 2 is shown in green. When the confidence is high (e.g., (a) and (d)) the behavior is more exploratory. As the certainty value is decreased (e.g., (b) and (e)), one may see that the action selection is increasingly clustered around the targets. When  $c$  is close to 0.0, the certainty is very low, so the planner will select points that obtain additional views of target (i.e., (c) and (f)). The number of times the robot views the target is counted and provided in the figure caption. The robots will select waypoints to fly over the targets more often as the uncertainty increases.

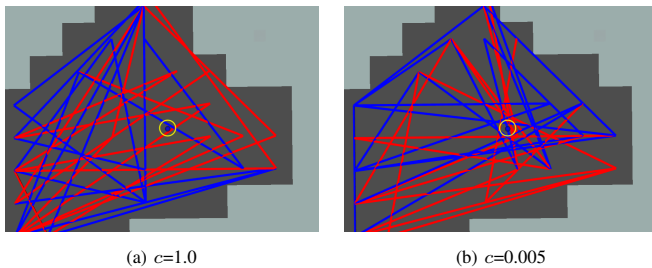


Fig. 8: Qualitative figure of the effect of varying the target uncertainty within the PX4 simulation stack. The target is outlined in a yellow circle. The trajectories in (a) explore the entire environment. In contrast, the trajectories in (b) are clustered around the target because of the high uncertainty. In this visualization, only, the cell sizes are  $30\text{ m} \times 30\text{ m}$ .

the GUTS approach slightly outperforms it. This is because the coverage planner stops running once all cells have been visited. However, the GUTS planner will continue revisiting areas. Because some of the cells along the border have a sliver of the cell inside the polygon, but not the center point, they will never be visited by the coverage planner. However, the GUTS planner will select paths that graze the boundary of the red zone and intersect with these cells. Therefore, the GUTS planner covers slightly more area than the coverage planner. For these simulation experiments, no objects of interest were included to enable a thorough analysis of the percent coverage achieved by each approach for the base case when nothing of interest is detected in the environment. Each cell is  $15\text{ m} \times 15\text{ m}$ , which is  $4\times$  smaller than what was used in [11].

Figure 6 provides the same analysis but with one object of interest, which is shown as a blue dot. The performance is similar to that shown in Fig. 5. Three robots are used in the simulation and the trajectories for each robot are shown in magenta, yellow, and cyan in Figs. 6c and 6d. The blue trajectories shown in Fig. 6d are the trajectories currently being executed. The white dots represent the robot's current position and the green dots represent the goal locations. These screenshots represent the state of the simulation at the end of the run, so the coverage planner had completed its search. The behavior of the GUTS approach is to first explore the environment without stopping even if it finds an uncertain target. When the environment is completely covered, it will re-fly over areas to obtain better views of the targets. This is demonstrated with qualitative simulation results in Figs. 7 and 8.

To evaluate the effect of target uncertainty, we vary the value of  $c$  and quantify the number of times the robot views the target(s).  $c$  is the only parameter varied in the simulations shown in Fig. 7. When the certainty is set to be high, the robot executes more exploratory behavior as shown in Figs. 7a and 7d. The 38 and 73 views, respectively, indicate the number of times the robots views the target(s). As the certainty is decreased, the number of views increases. This behavior is also mirrored in Fig. 8, which is a qualitative visualization of the behavior of a team of two robots operating within the PX4 simulation framework. The two robots pass over a target circled in yellow. When the

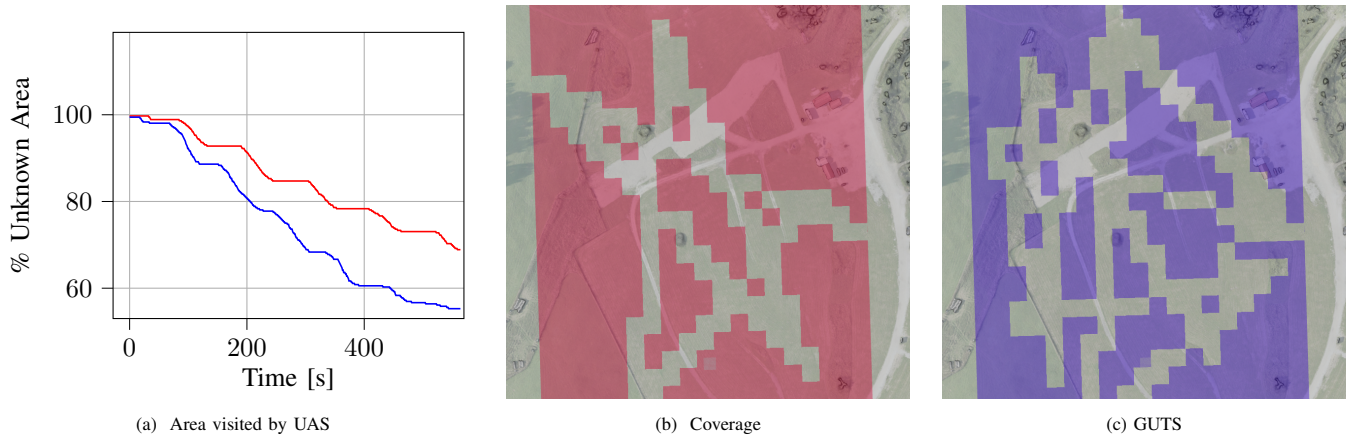


Fig. 9: The number of visited cells as a function of time illustrates the advantage of the decentralized GUTS approach compared to the naive coverage planner. Results obtained from flight data at the test site in Bloomingdale, OH. The flyable area for this experiment is 72 100 m<sup>2</sup>.

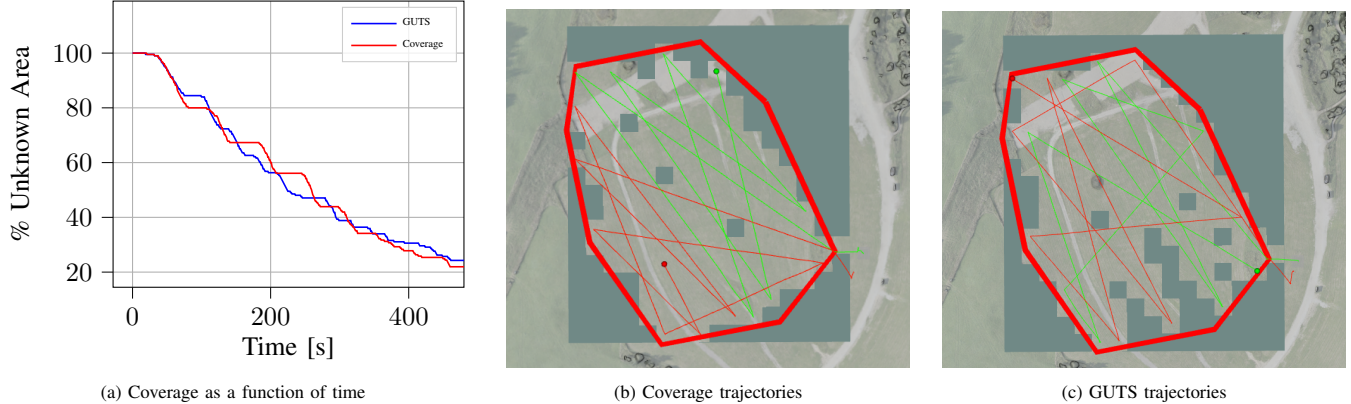


Fig. 10: The effect of enabling communication between robots is measured in this hardware experiment conducted at the test site in Bloomingdale, OH. Two robots are used for these experiments. Their trajectories are shown in red and green and their positions are shown as spheres. The explored area is shown as transparent cells, which enables the viewer to see the surface terrain. Unknown cells are gray-green and do not enable the viewer to see to the terrain below. The GUTS planner performs competitively with the greedy coverage planner. The flyable area for this experiment is 40 700 m<sup>2</sup>.

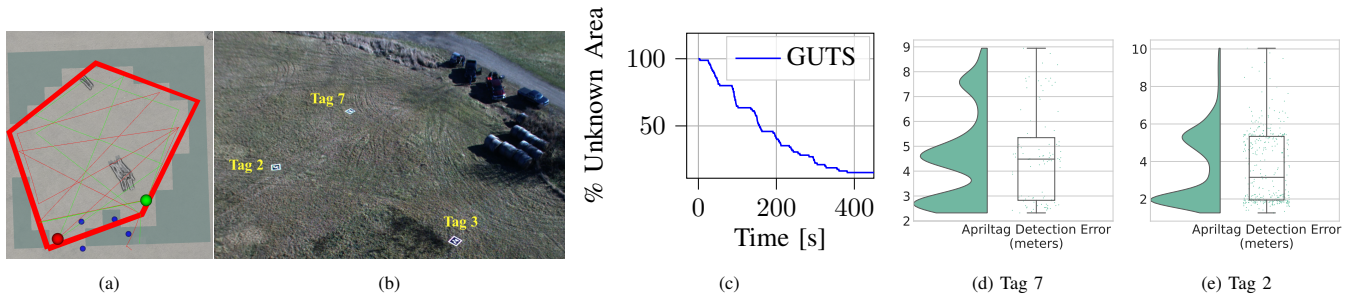


Fig. 11: For this hardware experiment, apriltags are added in the zone and communications are enabled between robots. (b) provides a visualization of the tag positions. Tags 2 and 4 are within the zone outlined in red in (a). The accuracy with which tags 7 and 2 are detected is shown in (d) and (e), respectively. The flyable area for this experiment is 15 000 m<sup>2</sup>.

uncertainty is high (as shown in Fig. 8b), the robots select trajectories that fly over the target.

### B. Hardware Results

To validate the simulations from Section V-A, the algorithms are deployed to hardware using the aerial vehicles described in Section IV-D. Three analyses are conducted to validate the simulations. All hardware tests were conducted in Bloomingdale, OH, a 1500+ acre site. An aerial view of the areas flown over during testing is shown in Fig. 4b.

The cell size used is 15 m × 15 m. The planners plan

continuously and the best action is stored. When time runs out, the best action is published. Due to our efficient C++ implementation, 100% of the cells are sampled and evaluated at each planning round. In contrast, 30 m × 30 m cell sizes and 0.0005% - 0.005% sampling is used by a single aerial system in [11].

The first hardware experiment evaluates the performance of the GUTS and coverage planners when communication is disabled with a team of two robots. Figure 9 provides quantitative analysis on hardware that validates the performance of the simulation. The valid flight area for both robots

is 72 100 m<sup>2</sup>, which is slightly smaller than the 75 000 m<sup>2</sup> used in [11]; however, we use 4× as many cells as they do to represent a given environment and we sample at 100% due to our efficient implementation. In these results, we see that that the GUTS planner outperforms the coverage planner when communication is denied. The advantage stems from the stochasticity of the GUTS planner. The areas visited by both robots are shown as transparent cells in Figs. 9b and 9c. The results demonstrate that the GUTS approach performs better when communications between the robots is denied.

The second hardware experiment evaluates the performance of the GUTS and coverage planners when communication is enabled. A team of two robots searches the areas shown in Figs. 10b and 10c. They share information about poses and goals; however, there are no objects to detect in the environment so no information about tracks is shared. Figure 10a illustrates the coverage as a function of time. We see that when communications between robots are enabled, the coverage approach performs similarly to the GUTS approach, which is in line with what we expect from the simulation results.

The last field test integrates targets and is shown in Fig. 11. Communication is enabled for this trial. These results correspond to the environment shown in Fig. 4c. The targets are shown as blue dots in Fig. 11a and labeled with their IDs in Fig. 11b. Tags 2 and 4 are contained within the boundary of the red zone. Tags 3 and 7 are detected on landing, but are outside the boundary of the red zone and are not included as a result. The error for two of the tags is shown in Figs. 11d and 11e. To localize the targets in the global coordinate frame, a ray from the camera is projected to the apriltag and intersected with a plane, which represents the environment. A plane is fit to the WingtraOne pointcloud data and used to perform the intersection. For this test a single trial is conducted with the GUTS planner. The track certainty is fixed to be low ( $c = 0.005$ ). Apriltags are used as targets because they are detected more reliably compared to neural-based object detectors. The performance of the GUTS planner is in line with the simulations.

## VI. CONCLUSION

This paper detailed a system and methodology for decentralized multi-robot active search and analyzed the performance while varying the availability of communications and target uncertainty. Future potential areas of research are to extend the implementation from 2D to 3D as well as consider terrain features where objects may be more likely to exist. Another interesting area of research is the development of a reward function that enables the robot to linger in uncertain regions and collect additional views before fully exploring the space. Increasing the number of coordinating robots presents opportunities for further improving the search performance. Robot assisted search holds the promise of safeguarding lives. To this end, we hope the results presented in this paper as well as open source software release accelerate innovation in this area and benefit the robotics community.

## VII. ACKNOWLEDGMENTS

This work was supported in part by the U.S. Army Research Office and the U.S. Army Futures Command under Contract No. W519TC-23-C-0031.

## REFERENCES

- [1] A. Hakami, A. Kumar, S. J. Shim, and Y. A. Nahleh, "Application of soft systems methodology in solving disaster emergency logistics problems," *International Journal of Industrial and Manufacturing Engineering*, vol. 7, no. 12, pp. 2470–2477, 2013.
- [2] R. Ashour, S. Aldhaheeri, and Y. Abu-Kheil, *Applications of UAVs in Search and Rescue*. Cham: Springer International Publishing, 2023, pp. 169–200. [Online]. Available: [https://doi.org/10.1007/978-3-031-32037-8\\_5](https://doi.org/10.1007/978-3-031-32037-8_5)
- [3] L. Franceschi-Bicchierai, "Officials search for 3 days; drone finds missing man after 20 minutes," Mashable, June 2014. [Online]. Available: <https://mashable.com/archive/drone-saves-life-missing-man>
- [4] O. Fernandes, R. Murphy, J. Adams, and D. Merrick, "Quantitative data analysis: Crasar small unmanned aerial systems at hurricane harvey," in *2018 IEEE International Symposium on Safety, Security, and Rescue Robotics (SSRR)*, 2018, pp. 1–6.
- [5] S. Saha, S. Nandi, P. S. Paul, V. K. Shah, A. Roy, and S. K. Das, "Designing delay constrained hybrid ad hoc network infrastructure for post-disaster communication," *Ad Hoc Networks*, vol. 25, pp. 406–429, 2015, new Research Challenges in Mobile, Opportunistic and Delay-Tolerant Networks Energy-Aware Data Centers: Architecture, Infrastructure, and Communication. [Online]. Available: <https://www.sciencedirect.com/science/article/pii/S1570870514001802>
- [6] A. Mpitzopoulos, D. Gavalas, C. Konstantopoulos, and G. Pantziou, "A survey on jamming attacks and countermeasures in wsns," *IEEE Communications Surveys & Tutorials*, vol. 11, no. 4, pp. 42–56, 2009.
- [7] F. Stache, J. Westheider, F. Magistri, C. Stachniss, and M. Popović, "Adaptive path planning for uavs for multi-resolution semantic segmentation," *Robotics and Autonomous Systems*, vol. 159, p. 104288, 2023.
- [8] E. Galceran and M. Carreras, "A survey on coverage path planning for robotics," *Robotics and Autonomous Systems*, vol. 61, no. 12, pp. 1258–1276, 2013. [Online]. Available: <https://www.sciencedirect.com/science/article/pii/S092188901300167X>
- [9] A. A. Meera, M. Popovic, A. Millane, and R. Siegwart, "Obstacle-aware Adaptive Informative Path Planning for UAV-based Target Search," in *2019 International Conference on Robotics and Automation (ICRA)*. Montreal, QC, Canada: IEEE, May 2019, pp. 718–724. [Online]. Available: <https://ieeexplore.ieee.org/document/8794345/>
- [10] J. Horyna, T. Baca, V. Walter, D. Albani, D. Hert, E. Ferrante, and M. Saska, "Decentralized swarms of unmanned aerial vehicles for search and rescue operations without explicit communication," *Autonomous Robots*, vol. 47, no. 1, pp. 77–93, 2023.
- [11] N. A. Bakshi, T. Gupta, R. Ghods, and J. Schneider, "Guts: Generalized uncertainty-aware thompson sampling for multi-agent active search," in *2023 IEEE International Conference on Robotics and Automation (ICRA)*, 2023, pp. 7735–7741.
- [12] R. Ghods, W. J. Durkin, and J. Schneider, "Multi-Agent Active Search using Realistic Depth-Aware Noise Model," Mar. 2021, arXiv:2011.04825 [cs, eess]. [Online]. Available: <http://arxiv.org/abs/2011.04825>
- [13] N. A. Bakshi and J. Schneider, "Stealthy Terrain-Aware Multi-Agent Active Search," Oct. 2023, arXiv:2310.10961 [cs]. [Online]. Available: <http://arxiv.org/abs/2310.10961>
- [14] D. Mellinger and V. Kumar, "Minimum snap trajectory generation and control for quadrotors," in *2011 IEEE International Conference on Robotics and Automation*, 2011, pp. 2520–2525.
- [15] M. W. Mueller, M. Hehn, and R. D'Andrea, "A computationally efficient motion primitive for quadcopter trajectory generation," *IEEE Transactions on Robotics*, vol. 31, no. 6, pp. 1294–1310, 2015.